Hyperfine Interact (2017) 238:56
DOI 10.1007/s10751-017-1422-x

Comparative study of the mechanical and tribological properties of a Hadfield and a Fermanal steel

P. C. Astudillo A.[1] · A. F. Soriano G.[1] · G. M. Barona Osorio[2] · H. Sánchez Sthepa[1] · J. Ramos[3] · J. F. Durán[2] · G. A. Pérez Alcázar[2]

Abstract In this study, Fe-12.50Mn-1.10C-1.70Cr-0.40Mo-0.40Si-0.50(max)P-0.50(max)S (Hadfield alloy) and Fe-28.4Mn-0.86C-1.63Al-0.42Cu-1.80Mo-1.59Si-0.60W (Fermanal alloy) (Wt. %) in the aged condition were compared in terms of its tribological and microstructural properties. The x-ray diffraction (XRD) patterns were refined with the lines of the austenitic γ-phase, Chromium Iron Carbide ($Cr_2Fe_{14}C$), Iron Carbide (Fe_2C), and Iron Oxide ($Fe_{0.974}O$ (II)) for the Hadfield alloy, and the lines of the austenitic γ-phase, martensite (M), $Mn_{1.1}Al_{0.9}$ phase and iron carbide (Fe_7C_3) for the Fermanal alloy. Mössbauer spectra were fit with two sites for the Hadfield alloy, which displayed as a broad singlet because of the austenitic disordered phase, and had a magnetic hyperfine field distribution, which corresponds to the $Cr_2Fe_{14}C$ ferromagnetic carbides found by XRD. There were two paramagnetic sites, a singlet, which corresponds to the austenite disordered phase, and a doublet, which can be attributed to the Fe_7C_3 carbide. The obtained Rockwell C hardness for aged Hadfield and Fermanal alloys were 43.786 and 50.018 HRc, respectively.

Keywords Hadfield steel · Fermanal steel · Mechanical properties · X-Ray diffraction · Mössbauer spectroscopy

This article is part of the Topical Collection on *Proceedings of the 15th Latin American Conference on the Applications of the Mössbauer Effect (LACAME 2016), 13–18 November 2016, Panama City, Panama*
Edited by Juan A. Jaén

✉ G. M. Barona Osorio
gisselle.barona@correounivalle.edu.co

[1] Escuela de Materiales, Universidad del Valle, A.A. 25360, Cali, Colombia

[2] Departamento de Física, Universidad del Valle, A.A. 25360, Cali, Colombia

[3] Universidad Autónoma de Occidente, Km. 2 vía Jamundí, Cali, Colombia

Published online: 15 May 2017

1 Introduction

In 1882, one of the first alloyed steels, manganese steel, which is composed of approximately 1.2% C and 12% Mn, was discovered by a metallurgist, Sir Robert Abbot Hadfield. The discovery of this steel is recognized as a landmark in metallurgical history, which was seen as the beginning of the age of alloy steels [1]. This alloy possesses properties such as high work hardening, high toughness, good ductility and wear resistance [2]. Currently, this steel is still widely used with some variations of its C and Mn compositions and the addition of alloying elements, such as chromium, vanadium, nickel, molybdenum, aluminum, nitrogen, among others [3]. The common compositions established by ASTM Standard A128 [4] for this steel allow for composition ranges from 1.0 to 1.4% C and from 10 to 14% Mn. Commercial alloys with manganese contents higher than 12% are seldom used because of their cost [5]. Hadfield steels have an austenitic microstructure after thermal treatment at temperatures higher than 500 °C, followed by a quench [6]. To modify the properties of Hadfield's steels, alloy elements are used. The combination of mechanical properties make Hadfield steels useful in many fields, and, it can be used in crawler treads for tractors, grinding mill liners, impact hammers and grinding mill liners [5].

After the development of Hadfield steels, other alloys based on the steel concept of this austenitic manganese steel with varying compositions followed [7]. One such alloy is the Fe-Mn-Al-C alloy or "Fermanal" steel, which was developed to replace some conventional stainless steels (Ni-Cr steels) [8]. This austenitic steel exhibit a good strain hardening behavior and is considered to be an economic substitutes for conventional austenitic stainless steels because it contains aluminum and manganese instead of chromium and nickel [9, 10]. In Fermanal steels, Mn levels between 28–47% stabilize the FCC austenitic phase, which improves their mechanical properties. G.L. Kayak [11] observed the carbon effects on the austenitic structure. An alloy with 30% Mn and 10% Al had an α-single-phase structure after quenching if it had 0.05% C and a two phase structure if it had 0.25% C. The level of α-phase decreases with increasing carbon; at 1% C, the structure was γ single-phase.

After thermally treating manganese steels, different combinations of mechanical stresses, fracture resistances and ductilities can be obtained, over a wide range of temperatures [10]. After casting, manganese steels are usually homogenized above 1050 °C to dissolve carbides; then, water quenching is used to provide a uniform austenitic structure [12]. J. Heredia [13] studied the influence of thermal treatment on the stability of the Hadfield steel austenite phase with 12% Mn. The specimens were heat treated at 1050 °C for two hours, followed by water quenching at room temperature. Some were subjected to heating stages from 100–500 °C, and exposed to plastic surface deformation. For all specimens, there was an austenitic matrix after austenizing, and it was demonstrated that the alloys retrained their mechanical properties when their surfaces were plastically deformed. In the absence of an inert atmosphere, a high solubilizing temperature often produces surface decarburization and leads to a loss of manganese, leading to the formation of α-martensite on the surface layer upon quenching [12]. The increase in the martensite content is good for increasing the mechanical properties of the steel [8].

Alloys pass through a series of decomposition reactions when they age. When aging occurs from 550 to 650 °C in Fermanal steels, carbides are distributed inside the austenitic matrix [11]. A. Prodhan and A. Chakrabarti [14] studied phase transformations during aging of Fe-Mn-Al-Si-C alloys that were treated at 1100 °C. They found precipitation of the Al(Fe,Mn)C_x phase inside the austenite grain when aged between 500–800 °C. J. Heredia [13] observed globular and transgranular acicular carbide precipitates in the

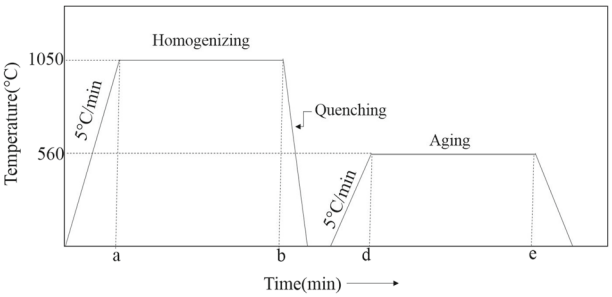

Fig. 1 Heat treatment cycle for Fermanal and Hadfield steels

austenitic grains at temperatures above 400 °C. The high mechanical properties of the alloy are due to the carbide precipitation inside the austenite [11, 14–16]. In this study, the results of the tribological and microstructural behavior of two Hadfield and Fe-Mn-Al-C alloyed steels under aged conditions are presented for comparison, establishing the performance of Fe-Mn-Al-C steel (unconventional steel) under the effects of wear. We aimed to evaluate whether Fe-Mn-Al-C is a good substitute for Hadfield steel (conventional steel).

2 Experimental procedure

Under the as-cast condition, Fe-12.50Mn-1.10C-1.70Cr-0.40Mo-0.40Si-0.50(max)P-0.50(max)S (Hadfield alloy) and Fe-28.4Mn-0.86C-1.63Al-0.42Cu-1.80Mo-1.59Si-0.60W (Fermanal alloy) (Wt%) were subjected to cutting, heat treatment, and etching for analysis. As-cast steels were cut in a rotating disc machine (MAXICUT). The samples were homogenized at 1050 °C for 5h, followed by quenching in a water and sodium chloride mixture (brine). The aging process was performed from room temperature to 560 °C, and the temperature was maintained for 5h. Figure 1 shows the heat treatment cycle for Fermanal and Hadfield steels. Metallographic specimens were etched with a 20% solution of nitric acid in ethanol for 15 s and a 4% solution of picric acid and ethanol for 20 s. The microstructures were characterized by using a Metallurgical Optical Microscope (MOM); also, the IQmaterials program was used to support the metallographic analysis performed. Scanning Electron Microscopy (SEM), X Ray Diffraction (XRD) with an X'Pert PRO PanAnalytical difractometer using the Kα lines of Cu and, Transmission Mössbauer Spectroscopy (TMS), using a 57Co (Rh) source and an α-Fe foil as the calibration sample. TMS spectra were taken from powder filled from the surface of the disk, and fit with the MOSFIT program [17]. The XRD patterns were refined with the GSAS program [18].

Hardness tests on the alloy surfaces were performed under aged conditions. Wilson Rockwell Hardness Tester was used to perform macro-hardness measurements under the ASTM E92 standard, and a Wilson microdurometer was used to perform micro-hardness measurements based on the ASTM E384 standard, wherein a 50 N indentation load and time of 15 s were used. A pin on disk tribometer (ASTM G99) was used for the wear resistance measurements. The ball specimen was Cr steel (diameter 6 mm) with an applied load of 3 and 10 N, sliding speed of 15 cm/s, and sliding distance of 1000m. The wear tests were performed at room temperature.

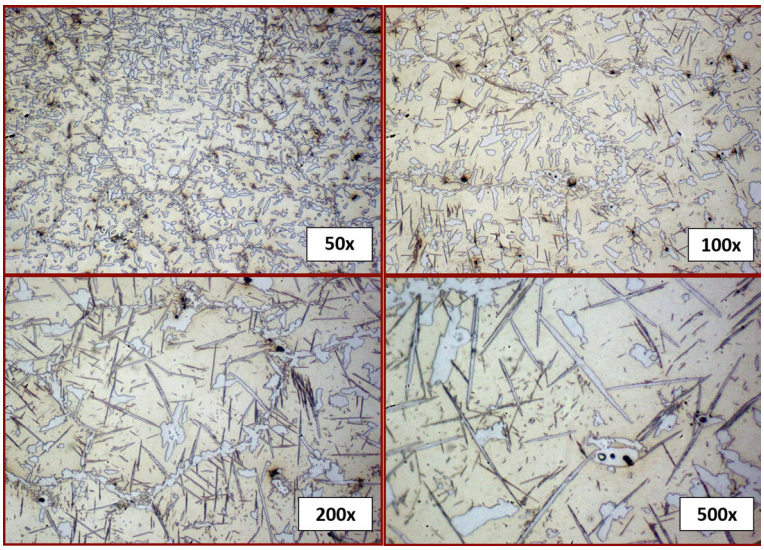

Fig. 2 Aged Hadfield alloy microstructures: **a** 50×, **b** 100×, **c** 200× and **d** 500×

3 Experimental results and discussion

Figure 2 shows micrographs of the aged Hadfield alloy taken at (a) 50×, (b) 100×, (c) 200×and (d) 500×. The aging time promoted the growth of acicular and irregular precipitates within the austenitic phase and formation of continuous precipitates at the grain boundaries. The areas of the austenitic phase and precipitates generated within the grains and at the boundaries were identified with the IQmaterials program, corresponding to 70.14% and 29.86%, respectively.

Figure 3 shows SEM images of the microstructure of the aged Hadfield alloy, and high precipitate levels on the surface and at the grain boundaries were observed, which contrast with the results obtained via Metallurgical Optical Microscopy. Table 1 shows the compositions spectra, in weight percent, found by Energy-dispersive X-ray spectroscopy (EDX). The Mn, Cr and Fe compositions did not significantly change, however, the carbon composition was higher in spectrum #1.

Figure 4 presents the XRD pattern of the aged Hadfield sample taken at room temperature. The pattern was refined with the lines of the austenitic γ-phase (A), Chromium Iron Carbide, $Cr_2Fe_{14}C$ (C_1), Iron Carbide, Fe_2C (C_2), and Iron Oxide, $Fe_{0.974}O$ (II) (O). Table 2 shows the spatial group, lattice parameters, weight proportion, and crystallite sizes obtained from the refinement of the observed phases. The weight proportions agreed with the results obtained by Metallurgical Optical Microscopy. The parallel and perpendicular crystallite sizes are the same for C_2 and for O, therefore, the crystallites are symmetric for these phases. Some parameters appear without error because they were fixed after a number of iterations.

Figure 5 shows the Mössbauer spectrum of powder obtained from the aged Hadfield sample. The powder was obtained after filling the surface of the sample with a diamond file. This spectrum was fitted with two sites: a broad singlet, which can be attributed to the austenitic disordered phase [19], and the magnetic hyperfine field distribution, which corresponds to the detected ferromagnetic carbides, as well as the XRD study, to the $Cr_2Fe_{14}C$ phase, which is iron rich, and to the Fe_2C phase, which is ferromagnetic [20, 21]. Some

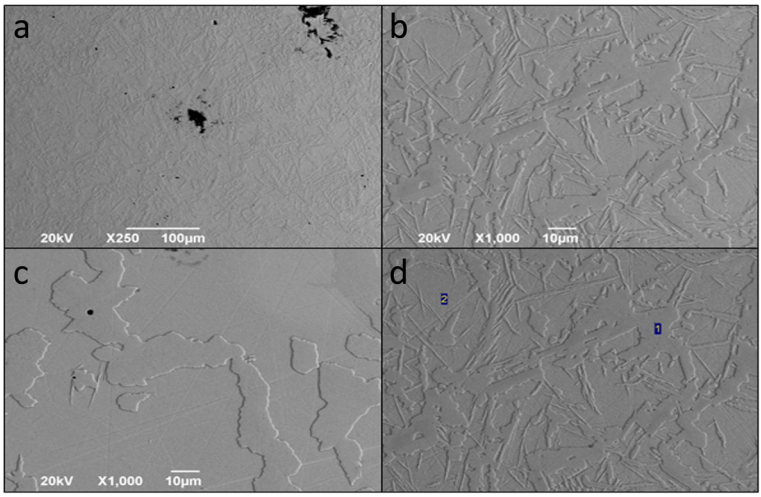

Fig. 3 Aged Hadfield alloy microstructures taken by SEM

Table 1 EDX composition spectra of the aged Hadfield sample

Spectrum	In stats	C	Si	Cr	Mn	Fe	Total
1	Yes	10.45	0.81	1.86	12.28	74.61	100.00
2	Yes	6.67	0.77	1.98	13.21	77.37	100.00
Max.		10.45	0.81	1.98	13.21	77.37	
Min.		6.67	0.77	1.86	12.28	74.61	

distribution fields are greater than others, which could be due to differences in Fe environments in the $Cr_2Fe_{14}C$ and Fe_2C phases. The iron oxide phase found by XRD could not be detected by Mössbauer spectrometry. We tried to insert the iron oxide phase into the spectrum as a doublet [22], however, it did not fit, showing that the iron fraction of this phase is lower than in the other two phases, or that this doublet is screened by the broad singlet of austenite. Table 3 shows the Mössbauer parameters obtained from the fit of the aged Hadfield sample. Some parameters appear without error because they were fixed.

Figure 6 shows the micrographs of the aged Fermanal alloy taken at (a) 50X, (b) 100X, (c) 200X, and (d) 500X. An austenitic structure with a continuous network of precipitates on the grain boundaries and globular precipitates inside the austenitic matrix are observed.

Figure 7 shows a SEM image of the microstructure of the aged Fermanal alloy, which had austenite grains with boundary precipitates. Table 4 shows the composition spectra determined by EDX, in weight percent, which were obtained at different points of Fig, 7. Spectrum #1 has 4.44% oxygen and 3.39% Al, therefore, an aluminum oxide or incrustation with manganese could be formed. Spectra #2, #3, #4 and #5 do not change much, however, the C and Al levels are high, and could be impurities inside the surface.

Figure 8 presents the XRD pattern of the aged Fermanal sample at room temperature. The pattern was refined with the lines of austenitic γ-phase (A), martensite (M), $Mn_{1.1}Al_{0.9}$ phase (M_1) and Iron Carbides, Fe_7C_3 (C). The spatial group, lattice parameters, weight proportion, and crystallite sizes obtained from the refinement of the observed phases are

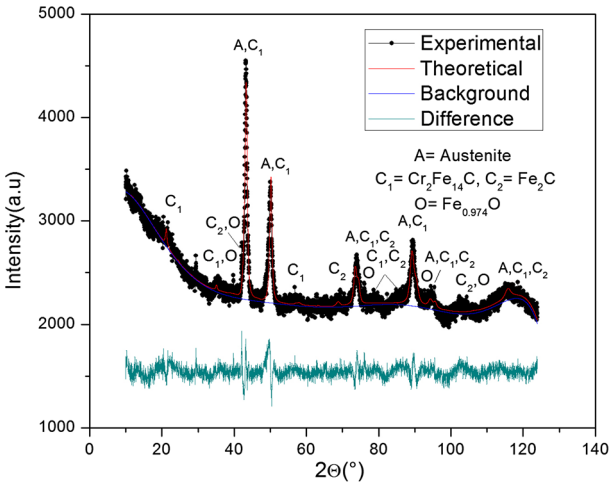

Fig. 4 XRD pattern of the aged Hadfield sample

Table 2 Structural parameters obtained from the refinement of the aged Hadfield sample

Phase	Spatial group	Lattice parameters			Weight proportion (%)	Crystallite sizes	
		a(Å) ±0.0002	b(Å) ±0.0002	c(Å) ±0.0002		Φ_{perp}(nm)	Φ_{paral}(nm)
Austenite	Fm3m	3.6479	3.6479	3.6479	63.001	94.07	93.60
$Cr_2Fe_{14}C$	Fm3m	7.2000	7.2000	7.2000	13.422±0.001	22.17	18.10
Fe_2C	Pnnm	4.2912	4.7171	2.7264	15.39±0.010	128.40	128.40
$Fe_{0.974}O$ (II)	R3m	3.0265	3.0265	7.5179	8.185	0.85	0.85

shown in Table 5. Crystallites are symmetric for the martensite phase. Some parameters appear to lack errors because they were fixed after a number of iterations.

Figure 9 shows the Mössbauer spectrum of the aged Fermanal sample. This spectrum was fit with a singlet, which corresponds to the austenite disordered phase, and a doublet, which can be attributed to the Fe_7C_3 carbide [23]. As observed in the spectra and in Table 6 the spectral area of the carbide is comparable to that of the austenite, as a result of the high Fe level in this phase. The disorder could be attributed to the quenching from high temperatures; in which the disordered austenite structure is frozen at a low temperature. The martensite phase detected by XRD, which is ferromagnetic, does not appear in the Mössbauer spectrum because its iron atoms content is lower than 2%. Some parameters appear to lack error because they were fixed.

The obtained Rockwell C hardness values for the aged Hadfield and Fermanal alloys were 43.786 and 50.018 HRc, respectively. This shows that the aging process allows for the formation of high hardness precipitates and a stable austenitic matrix. The difference between these values may be because the level of precipitates in the aged Hadfield alloy is higher, making this alloy more brittle than the aged Fermanal alloy. Figure 10 shows the areas to which the microhardness test was performed to the aged Hadfield alloy; the clear zone matrix (a) has an average hardness of 32.98 HRc; the precipitates generated at the

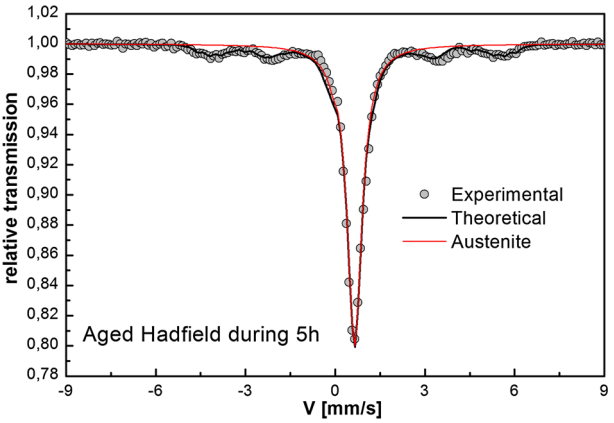

Fig. 5 Mössbauer spectrum of the aged Hadfield sample. The paramagnetic site corresponds to the austenite phase and the hyperfine magnetic field distribution corresponds to carbides

Table 3 Hyperfine interactions parameters obtained from the refinement of the aged Hadfield sample

Aged Hadfield	δ(mm/s)	Γ(mm/s)	ΔQ(mm/s)	H (kOe)	A (%)	Phase
Singlet	-0.131 ± 0.007	0.598 ± 0.004			81.24	Austenite + wüstite(?)
HMFD	-0.111	0.300	0.23 ± 0.05	287.29	18.76	$Cr_2Fe_{14}C + Fe_2C$

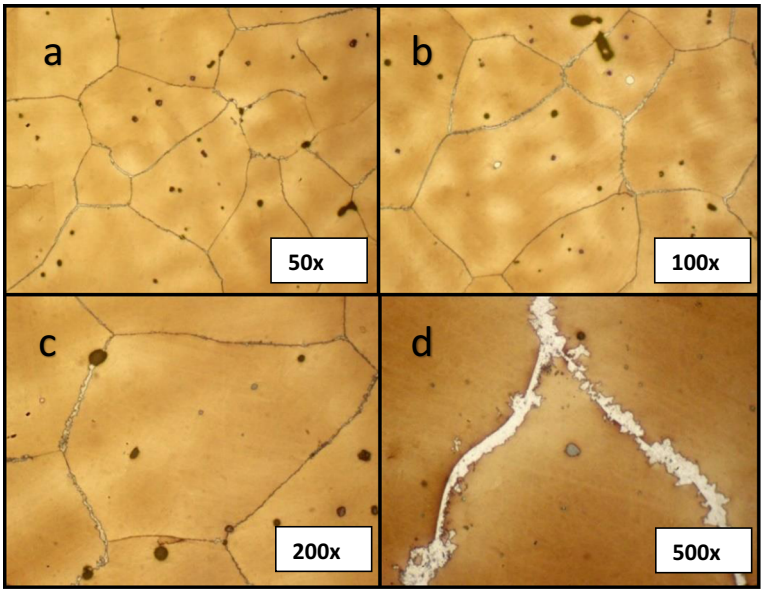

Fig. 6 Aged Fermanal alloy microstructures: **a** 50×, **b** 100×, **c** 200×, and **d** 500×

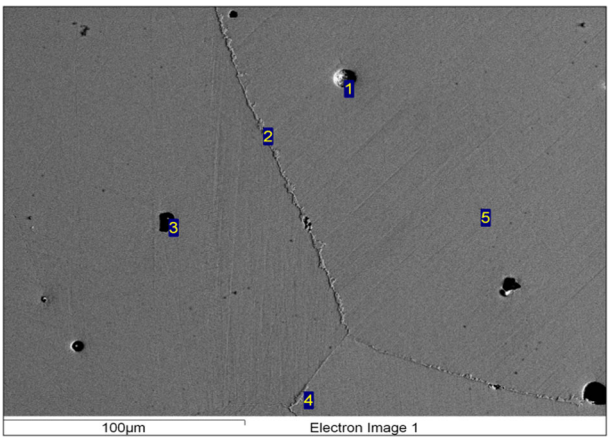

Fig. 7 Aged Fermanal alloy microstructures taken by SEM

Table 4 EDX composition spectra of the aged Fermanal sample

Spectrum	In stats	C	O	Al	Si	Mn	Fe	Total
1	Yes		4.44	3.93	1.36	27.86	62.41	100.00
2	Yes	7.38		4.31	1.93	26.91	59.47	100.00
3	Yes	8.54		5.45	1.62	24.93	59.46	100.00
4	Yes	8.02		5.04	1.88	26.12	58.94	100.00
5	Yes	8.44		4.95	1.90	25.46	59.24	100.00
Max.		8.54	4.44	5.45	1.93	27.86	62.41	
Min.		7.38	4.44	3.93	1.36	24.93	58.94	

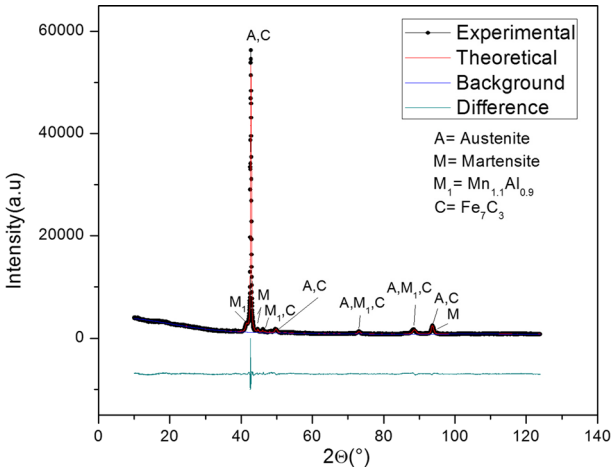

Fig. 8 XRD pattern of the aged Fermanal sample

Table 5 Structural parameters obtained from the refinement of the aged Fermanal sample

Phase	Spatial group	Lattice parameters			Weight proportion (%)	Crystallite sizes	
		a(Å) ±0.0002	**b(Å)** ±0.0002	**c(Å)** ±0.0002		Φ_{perp} (nm)	Φ_{paral} (nm)
Austenite	Fm3m	3.6597	3.6597	3.6597	76.382±0.001	12.14	121.38
Martensite	I4/mmm	2.8748	2.8748	3.0600	0.191	25.02	250.21
$Mn_{1.1}Al_{0.9}$	P4/mmm	2.7720	2.7720	3.4895	19.806	2.89	29.32
Fe_7C_3	Pnma	4.5364	6.8931	11.9112	3.983±0.003	34.56	15.36

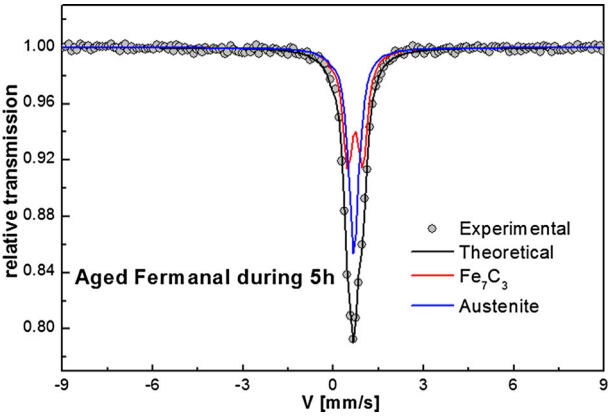

Fig. 9 Mössbauer spectrum of the aged Fermanal sample

grain boundaries (b) have higher microhardnesses than the matrix, with an average of 58.18 HRc; and the precipitates inside the austenite grains (c) have the highest average hardness of 61.81 HRc.

Figure 11 shows the areas to which the microhardness test were performed in the aged Fermanal alloy; austenite matrix has an average hardness of 49.9 HRc, while the grain boundary precipitates and precipitates inside the matrix had an average hardness of 66.1 HRc.

The samples were subjected to the pin on Disk tests at room temperature. For each load, three tests were performed to improve the statistical adjustment of the friction coefficient. For aged Hadfield samples with an applied load of 3 N in the stability zone the friction coefficient (FC) behavior was similar. For an applied load 10 N, many fluctuations were observed and the friction coefficient did not stabilize early. Sample #3 stabilized at 900m after a period of high fluctuations. One of the possible reasons for the fluctuations at the 10 N applied load is because the microstructure of aged Hadfield has a large portion of second phases or precipitates that would be expected to allow wear resistance. However, high loads can deform and break those phases forming hard shavings which would form a three-body system that would cause a high rate of wear on the material, and, therefore, a high friction coefficient. With a 3 N load applied to the aged Fermanal sample, friction coefficient stability was quickly reached. Only samples #1 and #2 were stabilized without fluctuations The sample #3 friction coefficient stabilized at 920 m. For the 10 N applied load,

Table 6 Hyperfine interactions parameters obtained from the refinement of the aged Fermanal sample

Aged fermanal	δ(mm/s)	ΔQ	Γ(mm/s)	A (%)	Phase
Doublet	0.050±0.049	0.501±0.006	0.201±0.012	49.75	Fe_7C_3
Singlet	−0.093±0.003	–	0.207±0.018	50.25	Austenite

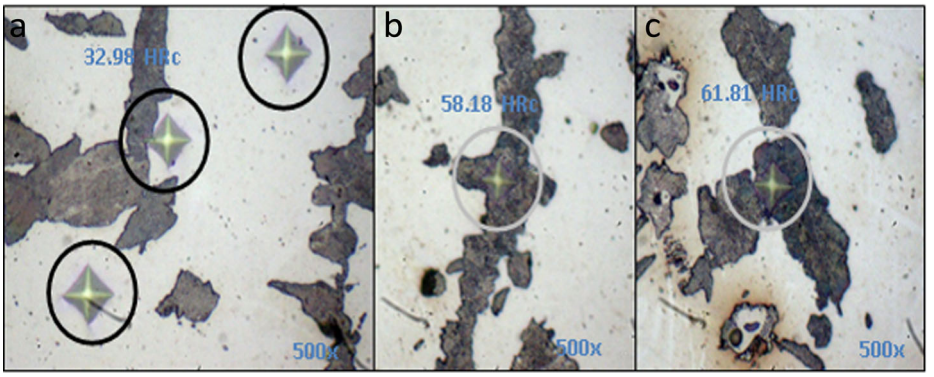

Fig. 10 Microhardness of the aged Hadfield phases

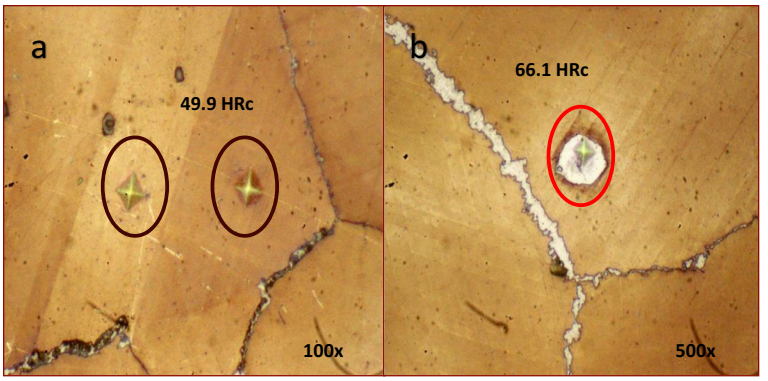

Fig. 11 Microhardness of the aged Fermanal phases

the time to stabilize was longer for the 3 samples. Because the stability zone did not have considerable fluctuations the friction coefficient was low and similar. The microstructure of the sample was harder and a low portion of precipitates caused tensions in the austenite

Table 7 Friction coefficient obtained from the Pin on Disk tests

Type	Applied Load	Sample	Max friction coefficient	Average steady state sliding friction coefficient	Average friction coefficient
Aged Hadfield	3N	1	0.5013	0.4610	0.4603
		2	0.6270	0.4520	
		3	0.6040	0.4680	
	10N	1	0.7220	0.6420	0.594
		2	0.7590	0.6500	
		3	0.8390	0.4900	
Aged Fermanal	3N	1	0.6327	0.3989	0.4349
		2	0.4159	0.3949	
		3	0.5370	0.4868	
	10N	1	0.7344	0.4190	0.4266
		2	0.6570	0.4060	
		3	0.7300	0.4550	

crystalline structure. The maximum friction coefficient and average steady state sliding friction coefficient are shown in Table 7 for both the Hadfield and Fermanal samples.

4 Conclusions

According to the results, the mechanical properties of Fermanal steel, such as hardness, micro hardness and wear resistance, are better than those of Hadfield steel. Carbide precipitation and martensite transformation were observed in Fermanal steel, while only the first was observed in Hadfield steel. This can be interpreted as a consequence of the thermal treatments, which produce martensite in the Fermanal sample, and this phase improves the mechanical properties of steel. The wear test on Fermanal steel increases the martensite fraction, improving its mechanical properties, as reported by Ramos et al. [8].

Acknowledgments The authors would like to thank Universidad del Valle, to Colciencias under contract No. FP44842-032-2016, and to CENTRO DE EXCELENCIA EN NUEVOS MATERIALES, CENM, for research financial support.

References

1. Tweedale, G.: Sir Robert Abbott Hadfield F.R.S. (1858-1940), and the discovery of manganese steel. Notes Rec. R. Soc. **40**, 63 (1985)
2. Srivastava, A., Das, K.: Microstructural characterization of Hadfield austenitic manganese steel. Mater. Sci. **43**, 5654 (2008)
3. Valencia, A.: LAS POSIBILIDADES DE UN NUEVO ACERO Fe–Mn–Al–Si. Rev. Colomb. Mater. **7**, 1 (2012)
4. ASTM A128/A128M-93 Standard Specification for Steel Castings, Austenitic manganese american society for testing and materials (2012)

5. Dastur, Y.N., Leslie, W.C.: Mechanism of work hardening in Hadfield manganese steel. Metall. Trans. A **12**, 749 (1981)
6. García, A., Varela, Á., Mier, J.L., Camba, C., Barbadillo, F.: Estudio tribológico de aceros austenticos tipo Hadfield: influencia del manganeso en su respuesta frente al desgaste. Rev. Metal. **46**, 47 (2010)
7. Hofer, S., Hartl, M., Schestak, G., Schneider, R., Arenholz, E., Samek, L.: Comparison of austenitic High-Mn-Steels with different Mn- and C-contents regarding their processing properties. BHM Berg-und Hüttenmännische Monatshefte **156**, 99 (2011)
8. Ramos, J., Piamba, J.F., Sánchez, H., Pérez Alcazar, G.A.: Mössbauer and XRD characterization of the phase transformations in a Fe-Mn-Al-C-Mo-Si-Cu as cast alloy during tribology test. Hyperfine Interact. **232**, 119 (2015)
9. Kim, H., Suh, D., Kim, N.J.: Fe–Al–Mn–C lightweight structural alloys: a review on the microstructures and mechanical properties Sci. Technol. Adv. Mater. **14**, 017205 (2013)
10. Ramos, J.: Obtención siderúrgica y aplicación industríal de los aceros fermanal: Fe-28,6Mn-5,63A1-0.86C-0.43Cu-1,81Mo-1,59Si-0,60W Y Fe-28,6Mn-1,60A1-0.86C-0.43Cu-1,81Mo-1,59Si-0,60W, Ph.D thesis (2011)
11. Kayak, G.L.: Fe–Mn–Al precipitation-hardening austenitic alloys. Met. Sci. Heat Treat. **11**, 95 (1969)
12. Sant, S.B., Smith, R.W.: A study in the work-hardening behaviour of austenitic manganese steels. J. Mater. Sci. **22**, 1808 (1987)
13. Heredia, J.C.: Estabilidad de la fase austenítica, variación de la dureza en los aceros al manganeso afectados por el calor y sometidos a impactos. Rev. Del Inst. Investig. (RIIGEO), UNMSM **15**, 99 (2012)
14. Prodhan, A., Chakrabarti, A.: A study on age hardening in cast Fe-Mn-Al-Si-C alloys. J. Mater. Sci. **25**, 1856 (1990)
15. Sato, K., Tagawa, K., Inoue, Y.: Spinodal decomposition and mechanical properties of an austenitic Fe-30wt.%Mn-9wt.%Al-0.9wt.%C alloy. Mater. Sci. Eng. A **111**, 45 (1989)
16. Sato, K., Tagawa, K., Inoue, Y.: Age hardening of an Fe-30Mn-9Al-0.9C alloy by spinodal decomposition. Scr. Metall. **22**, 899 (1988)
17. Varret, F., Teillet, J.: Unpublished MOSFIT program
18. Larson, A.C., Von Dreele, R.: General structure analaysis system (GSAS), los alamos national laboratory report, LAUR, 86 (2004)
19. Paduani, C., Galvão, E., Pérez Alcazar, G.A.: Mössbauer effect study of γ-FeMn alloys. Hyp. Int. **73**, 233 (1992)
20. Johnston, W.D., Heikes, R.R., Petrolo, J.: The preparation of fine powder hexagonal Fe2C and its coercive force. J. Phys. Chem. **64**(11), 1720 (1960)
21. Silva de Oliveira, L.: Ph. D. Thesis, UFMG, Porto Alegre, Brazil (1991)
22. Moya, T., Fournès, L., Hagenmuller, P., Kolditz, L., Blumenthal, G., Wegner, G.: Mößbauer-Untersuchung der thermischen Umwandlungen von Kaolin Caminau im Temperaturbereich 383K bis 1465 K. Z. Chem. **25**(9), 343 (1985)
23. Bavinov, V.A., Tsurin, V.A., Surikov, V.T.: Study of mechanically synthesized carbide Fe7C3. Phys. Metals. Matallogr. **110**, 474 (2010)